Title	Finite Deformation Analysis of Dynamic Behavior of Embankment on Liquefiable Sand Deposit Considering Pore Water Flow and Migration
Author(s)	Ueda, K.; Iai, S.; Ozutsumi, O.
Citation	The 6ICEGE Proceedings (2015)
Issue Date	2015
URL	http://hdl.handle.net/2433/230373
Right	The organizer of '6ICEGE' approved uploadong the files into this repository.
Type	Conference Paper
Textversion	publisher

6ICEGE
6th International Conference on Earthquake Geotechnical Engineering
1-4 November 2015
Christchurch. New Zealand

Finite Deformation Analysis of Dynamic Behavior of Embankment on Liquefiable Sand Deposit Considering Pore Water Flow and Migration

K. Ueda[1], S. Iai[2], O. Ozutsumi[3]

ABSTRACT

To verify the applicability of a finite deformation analysis considering pore water flow using a strain space multiple mechanism model based on Total Lagrangian (TL) and Updated Lagrangian (UL) formulations, seismic response analyses are performed on the dynamic behavior of an embankment considering aftershocks after a main shock. Comparison between the experimental and analytical results indicated that the time history of excess pore water pressure was well simulated by considering the pore water drainage during computation. In addition, the results (e.g., the crest settlement, deformed configuration, and acceleration response) obtained in the finite deformation analyses based on both TL and UL formulations were in good agreement with the measurement. In conclusion, in order to accurately predict the behavior of embankment during and after large earthquakes, including aftershocks, it is required to take into account the effect of both geometrical nonlinearity and pore water flow and migration.

Introduction

A finite element program “FLIP (Finite Element Analysis Program of Liquefaction Process)” is a computer program for dynamic effective stress analysis of soil-structure systems during earthquakes including soil liquefaction. In the program, a strain space multiple mechanism model called “Cocktail glass model” proposed by Iai et al. (2011) is introduced to the simulation considering pore water flow and migration and begins to be used for seismic design these days. However, the formulation of the model has been carried out based on the infinitesimal strain theory, which means that the application should be limited to phenomena under small strain, displacement and rotation. Therefore, the authors have extended the Cocktail glass model based on finite strain theory, including both total and updated Lagrangian formulations, to simulate large strain and rotation phenomena (Iai et al., 2013) and a finite strain analysis program called “FLIP/TULIP (Total and Updated Lagrangian Program of Liquefaction Process)” has been developed by introducing the extended model. However, the finite strain program couldn’t take into account the drainage effect of pore water and the applicability is limited to the simulation under undrained condition. The drainage effect can’t be ignored when considering a seismic response under a long-duration earthquake and/or aftershocks following a main shock (Ueda et al., 2014). This is why the program has been updated to consider the effect of pore water flow and migration with geometrical nonlinearity simultaneously. In this research, the performance of the program is studied by simulating the dynamic behavior of embankments on liquefiable sand deposits considering aftershocks in order to verify the applicability of the program.

[1]Assistant Professor, DPRI, Kyoto University, Uji, Kyoto, Japan, ueda.kyohei.2v@kyoto-u.ac.jp
[2]Professor, DPRI, Kyoto University, Uji, Kyoto, Japan, iai.susumu.6x@kyoto-u.ac.jp
[3]President, Meisosha Co., Toshima-ku, Tokyo, Japan, ozutsumi@meisosha.co.jp

Summary of Centrifuge Model Test

A series of centrifuge model tests was performed in the P.W.R.I (2000) to study the dynamic behavior of an embankment on a liquefiable sand deposit. The applied centrifugal acceleration was 50 G. In the experiments, various sorts of remedies were adopted to prevent the settlement of an embankment. In this research, the target of the simulation is the result of the test case with no remedies. A model configuration shown in Fig. 1 is a cross section of an embankment on the sand deposit with 13.0 m depth. The crest height is 5.0 m, and lateral length at the top and bottom are 3.0 m and 23.0 m, respectively. The groundwater level is at 1.8 m below the surface of the ground. The relative density of the upper layer and lower layer of the saturated sand deposit is approximately 60 % and 90 %, respectively. Figure 2 shows the input motion, which is composed of seven sinusoidal waves (main shock) with a peak acceleration of approximately 0.4 g and subsequent aftershocks with acceleration amplitudes less than 0.1 g. The induced crest settlement was 2.04 m and 2.30 m at the end of the main shock and aftershocks, respectively.

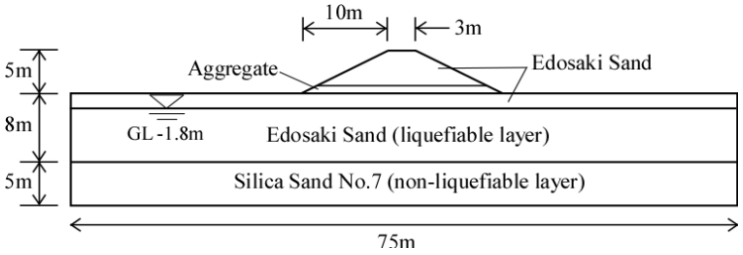

Figure 1. The cross-section diagram in centrifuge model test (Modified after P.W.R.I. (2000))

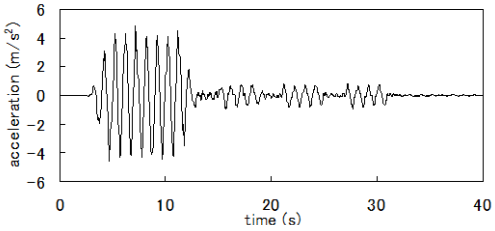

Figure 2. Input acceleration (P.W.R.I. (2000))

Constitutive Model of Soils

Cocktail Glass Model Based on Infinitesimal Strain Theory

The effective stress model of sands to be used in this study is a strain space multiple mechanism model called “Cocktail glass model”, in which a new stress-dilatancy relationship is introduced (Iai et al., 2011). The integrated form of the constitutive relation is given by

$$\boldsymbol{\sigma}' = -p\mathbf{I} + \sum_{i=1}^{I} q^{(i)} \left\langle \mathbf{t}^{(i)} \otimes \mathbf{n}^{(i)} \right\rangle \Delta\omega, \quad \left\langle \mathbf{t}^{(i)} \otimes \mathbf{n}^{(i)} \right\rangle = \mathbf{t}^{(i)} \otimes \mathbf{n}^{(i)} + \mathbf{n}^{(i)} \otimes \mathbf{t}^{(i)} \tag{1}$$

where $\boldsymbol{\sigma}'$ and $\boldsymbol{\varepsilon}$ denote effective stress and strain tensors, $p = p(\varepsilon')$ denotes effective confining pressure, $\mathbf{I}$ is the second order identity tensor, $q = q(\gamma,\ \varepsilon',\ \varepsilon'')$ denotes virtual simple shear stress, $\mathbf{n}$ denotes a unit vector along the direction of the branch between particles, $\mathbf{t}$ is a unit vector normal to $\mathbf{n}$. The virtual simple shear strain γ and the effective volumetric strain ε' are defined introducing the effect of volumetric strain due to dilatancy $\varepsilon_{\mathrm{d}} \left(= \varepsilon_{\mathrm{d}}^{\mathrm{c}} + \varepsilon_{\mathrm{d}}^{\mathrm{d}}\right)$ and as follows:

$$\gamma^{(i)} = \left\langle \mathbf{t}^{(i)} \otimes \mathbf{n}^{(i)} \right\rangle : \boldsymbol{\varepsilon} \quad \text{and} \quad \varepsilon' = \varepsilon - \varepsilon_{\mathrm{d}} \tag{2}$$

where $\varepsilon_{\mathrm{d}}^{\mathrm{c}}$ and $\varepsilon_{\mathrm{d}}^{\mathrm{d}}$ indicate the contractive and dilative components of dilatancy (Iai et al., 2011).

Finite Strain Formulation of Cocktail Glass Model in Reference Configuration

The strain space multiple mechanism model described in the previous section has been extended based on finite strain formulation (Iai et al., 2013). In the formulation, the unit vector **N** along the direction of the branch and the unit vector **T** normal to **N** are defined in the reference configuration. These vectors are assumed to change their direction and magnitude into $\mathbf{n}=\mathbf{F}\mathbf{N}$ and $\mathbf{t}=\mathbf{F}\mathbf{T}$ in the current configuration through the deformation gradient $\mathbf{F}\left(=\partial\mathbf{x}/\partial\mathbf{X}\right)$. The material description of integrated form of the strain space multiple mechanism model in the reference configuration is given in terms of the second Piola-Kirchhoff effective stress $\mathbf{S}'$ using the relations of $J=\det\mathbf{F}$, $\mathbf{C}=\mathbf{F}^{\mathrm{T}}\mathbf{F}$ and the fourth-order unit tensor ¥ as follows:

$$\mathbf{S}'=-Jp\mathbf{C}^{-1}+J^{-1}\mathbf{Q}:\bar{\mathbf{S}},\ \text{where}\ \mathbf{Q}=¥-\mathbf{C}^{-1}\otimes\mathbf{C}/2\ \text{and}\ \bar{\mathbf{S}}=\sum_{i=1}^{I}Jq^{(i)}\left\langle\mathbf{T}^{(i)}\otimes\mathbf{N}^{(i)}\right\rangle\Delta\omega \tag{3}$$

By taking the material time derivative of both sides of Equation (3), the incremental form of the constitutive equation in the reference configuration is derived (see Iai et al., 2013).

Finite Strain Formulation of Cocktail Glass Model in Current Configuration

The spatial description of integrated form in the current configuration is obtained in terms of the Cauchy effective stress $\boldsymbol{\sigma}'$ through the push-forward operation of Equation (3) as follows:

$$\boldsymbol{\sigma}'=-p\mathbf{I}+J^{-1}\mathbf{Z}:\bar{\boldsymbol{\sigma}},\ \mathbf{Z}=¥-\mathbf{I}\otimes\mathbf{I}/2\ \text{and}\ \bar{\boldsymbol{\sigma}}=\sum_{i=1}^{I}q^{(i)}\left\langle\mathbf{t}^{(i)}\otimes\mathbf{n}^{(i)}\right\rangle\Delta\omega \tag{4}$$

By taking the Lie time derivative of both sides of Equation (4), the incremental form of the constitutive equation in the current configuration is derived (see Iai et al., 2013).

Governing Equations of Porous Saturated Materials

The equilibrium and mass balance of porous saturated materials are briefly reviewed in the context of finite strain formulation. The spatial description of the governing equations of the boundary value problems of porous materials is given in terms of Cauchy total stress $\boldsymbol{\sigma}$, displacement $\mathbf{u}$ and pore water pressure p as follows (Zienkiewicz and Bettess, 1982):

$$\begin{aligned}&\mathrm{div}\boldsymbol{\sigma}(\mathbf{x},t)+\rho(\mathbf{x},t)\mathbf{g}(\mathbf{x})=\rho(\mathbf{x},t)\ddot{\mathbf{u}}(\mathbf{x},t)\\&\mathrm{div}\left(\mathbf{k}(\mathbf{x})\mathrm{grad}\left(p(\mathbf{x},t)\right)\right)-\mathrm{div}\dot{\mathbf{u}}(\mathbf{x},t)-\mathrm{div}\left(\mathbf{k}(\mathbf{x})\rho_{\mathrm{f}}(\mathbf{x},t)\mathbf{g}(\mathbf{x})\right)=-\mathrm{div}\left(\mathbf{k}(\mathbf{x})\rho_{\mathrm{f}}(\mathbf{x},t)\ddot{\mathbf{u}}(\mathbf{x},t)\right)+n\dot{p}(\mathbf{x},t)/K_{\mathrm{f}}\end{aligned} \tag{5}$$

where ρ and ρ_{f} denote bulk and fluid density, $\mathbf{g}$ is acceleration of gravity, $\mathbf{k}$ denotes permeability tensor, K_{f} denotes bulk modulus of pore fluid and n is porosity. By using the definition of effective stress ($\boldsymbol{\sigma}=\boldsymbol{\sigma}'-p\mathbf{I}$), the equilibrium equation in Equation (5) is rewritten

as follows:

$$\int_{\Omega}\left[\left(\boldsymbol{\sigma}'-p\mathbf{I}\right):\delta\mathbf{e}-(\rho\mathbf{g}-\rho\ddot{\mathbf{u}})\cdot\delta\mathbf{u}\right]\mathrm{d}v-\int_{\partial\Omega_{\sigma}}\bar{\mathbf{t}}\cdot\delta\mathbf{u}\mathrm{d}s=0 \tag{6}$$

The above equation is transformed into the reference configuration through the pull-back operation as follows:

$$\int_{\Omega_0}\left[\left(\mathbf{S}'-Jp\mathbf{C}^{-1}\right):\delta\mathbf{E}-(\rho_0\mathbf{g}-\rho_0\ddot{\mathbf{u}})\cdot\delta\mathbf{u}\right]\mathrm{d}V-\int_{\partial\Omega_{0\sigma}}\bar{\mathbf{T}}\cdot\delta\mathbf{u}\mathrm{d}S=0 \tag{7}$$

Similarly the mass balance equation of fluid is rewritten through the Galerkin method in the current and reference configuration (Ueda, 2009). The equations for the current configuration gives the formulation of the updated Lagrangian (UL) method, while those for the reference configuration gives the formulation of the total Lagrangian (TL) method.

Outline of Finite Element Analysis

Determination of Model Parameters

The strain space multiple mechanism model has 15 parameters for the analysis of liquefaction; three specify volumetric mechanism, three specify shear mechanism, and the rest control liquefaction and dilatancy. The parameters for defining the characteristics of volumetric and shear deformation, which were determined by reference to the past study (Hyodo et al., 2008) are shown in Table 1. The permeability of the saturated layers, which is required for the simulation considering pore water flow and migration, is determined based on the results of permeability tests (Yoshizawa et al., 2009). The rest parameters that specify the characteristics of liquefaction and dilatancy are shown in Table 2. These parameters were determined by referring to the liquefaction resistance curves which were obtained from the cyclic triaxial tests under the undrained condition. Figure 3 shows measured and computed liquefaction resistance curves. The parameter q_{us} in Table 2, which is the undrained shear strength for describing the steady state of sand, was determined for the Edosaki sand from the void ratio and fines content following Motoshima et al. (2008). The parameter is not defined for the silica sand, whose fines content is only 0.7%, because the undrained shear strength for clean sands becomes very large in general.

Table 1. Model parameters for deformation characteristics

Soil Type		density ρ (t/m^3)	porosity n	permeability k (m/s)	Parameters for deformation characteristics					
					volumetric mechanism			shear mechanism		
					K_{ma}(kPa)	r_K	l_K	G_{ma}(kPa)	φ_{f}(°)	$h_{\max}$
Edosaki sand	embankment	1.70	0.49	-	218000	-	-	84000	34.0	0.26
	dry	1.68	0.49	-	107000	-	-	41000	34.0	0.26
	saturated	1.86	0.49	1.95×10^{-3}	107000	0.5	2.0	41000	34.0	0.26
silica sand	saturated	1.98	0.40	1.00×10^{-3}	224000	0.5	2.0	86000	48.0	0.24

(σ_{ma}'=98.0kPa)

Table 2. Model parameters for dilatancy

Soil Type	Parameters for dilatancy (only for saturated layers)								
	φ_p (°)	ε_d^{cm}	$r_{\varepsilon_d^c}$	r_{ε_d}	q_1	q_2	S_1	c_1	q_{us} (kPa)
Edosaki sand	28.0	0.15	4.00	0.50	1.00	0.50	0.005	1.75	17.0
silica sand	33.0	0.10	1.00	0.12	1.00	1.10	0.005	1.45	-

Initial and Boundary Conditions and Input Motion

The numerical analysis was carried out with the same prototype dimension of the centrifuge model test. In order to replicate the boundary conditions of the rigid container in the test, degrees of freedom of displacements at the base were fixed both horizontally and vertically, and only horizontal displacements were fixed at the side boundaries as shown Fig. 4. Pore water pressure was specified as zero at the groundwater level. A seismic response analysis was performed for 50 s considering pore water flow following a self-weight analysis. The recorded motion including aftershocks (Fig. 2) at the bottom of the container was used as an input motion. The numerical time integration was done by the SSpj method using a time step of 0.01 s. Rayleigh damping (α=0.0, β=0.0002) was used to ensure stability of the numerical solution process.

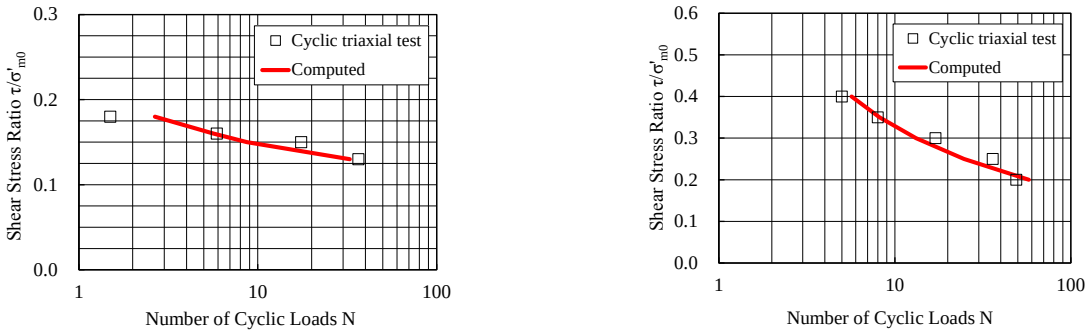

(a) Edosaki sand (b) silica sand

Figure 3. Liquefaction resistance curves

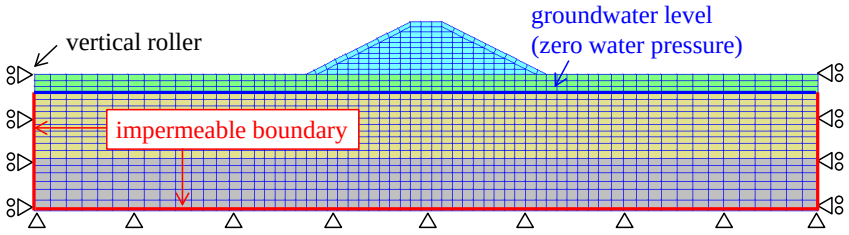

Figure 4. Finite element mesh for numerical analysis

Results of the Analysis

Computed Deformation of the Embankment

Figure 5 shows measured and computed residual deformations of the embankment after the dissipation of excess pore water pressure (E.P.W.P.). The deformations are shown by deformed meshes in solid lines with reference to the original configuration in broken lines. Figure 5 (a) indicates that the deformed configuration obtained in the infinitesimal strain analysis differs from the measured one shown in Fig. 5 (d). The shape of the embankment becomes flat and the residual height is almost equal to that of the surrounding ground. The time history of the crest settlement is shown in Fig. 6, which indicates that the infinitesimal deformation analysis overestimates the amount of the settlement approximately as 1.5 times as the measurement throughout the computation. Figures 5 (b) (c) and 6 indicate that the results obtained in the finite strain analyses are in good agreement with the measurement. In both the measured and computed shapes, soils near the toes of the embankment are laterally expanded in the direction opposite to the embankment, while soils under the embankment are compressed vertically and sheared. The computed deformation mode is characterized by a crest settlement associated with lateral spread in the foundation soils as the measured one is. In addition, no significant difference is recognized in the deformed shape and the time history of the settlement between TL and UL formulation. These results indicate that the Cocktail glass model, which has been extended based on the finite strain formulation, shows a reasonable capability to reproduce the deformation of an embankment irrespective of which formulation is used.

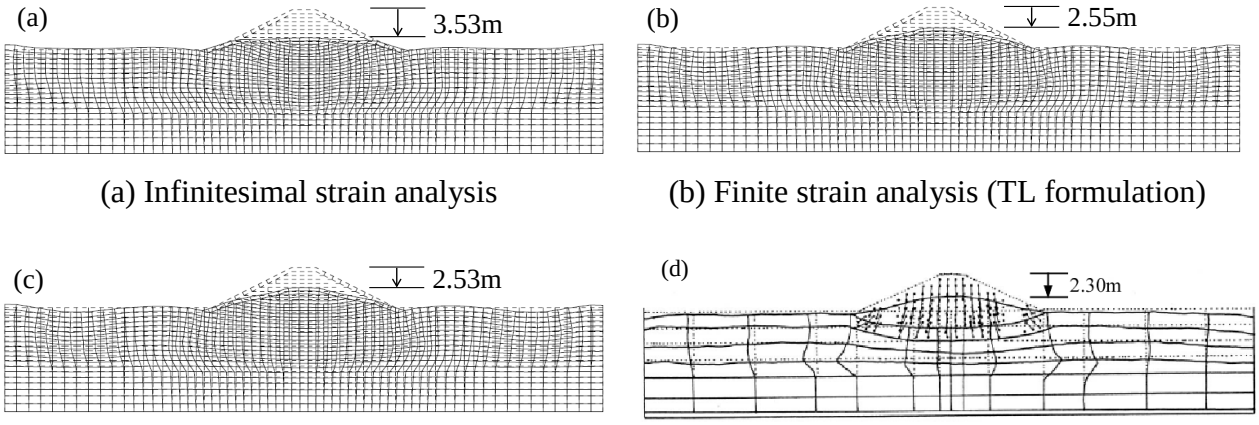

(a) Infinitesimal strain analysis (b) Finite strain analysis (TL formulation)

(c) Finite strain analysis (UL formulation) (d) Measured

Figure 5. Computed and measured residual deformation

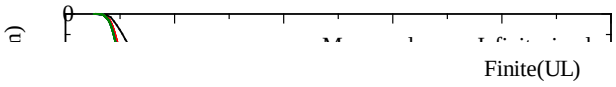

Figure 6. Time history of the crest settlement

Variation of Peak Acceleration with Depth

Vertical arrays of the peak amplitude of horizontal acceleration are shown in Fig. 7. In the centrifuge model test, the acceleration in the liquefiable deposit are more or less attenuated and not amplified due to partial liquefaction. The variation at the center axis of the embankment indicates that the strong attenuation of the acceleration amplitude in a shallow layer prevents the wave propagation to the embankment. Figure 7 indicates that the computed variation on the surrounding ground is identical to the measurement, regardless of whether the geometrical nonlinearity is considered or not. While the finite strain analyses show good agreement with the measurement near the shallow liquefiable layer at the toe of the embankment compared to the infinitesimal strain analysis, the opposite tendency is recognized at the center axis of the embankment. Although the measured variation can't be completely simulated by the finite strain analyses and further studies seem to be required about this cause, the overall tendency of the peak acceleration profile is considered to be well simulated.

Variation and Time History of Excess Pore Water Pressure

The vertical array of the maximum E.P.W.P. is shown in Fig. 8. Regardless of whether the geometrical nonlinearity is considered or not, the measured vertical profile is well simulated, in particular at the surrounding ground where the E.P.W.P. builds up and becomes equal to the initial vertical effective stress, which indicates the occurrence of full liquefaction. Although the

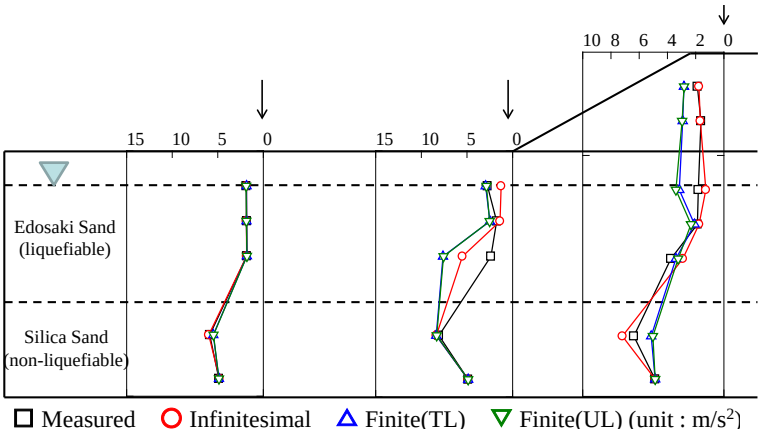

Figure 7. Variation of peak amplitude of acceleration in depth

maximum value at the center axis of the embankment, in which the E.P.W.P. rises up to some extent but liquefaction doesn't occur, is a little overestimated in both the infinitesimal and finite strain analyses, the finite strain analyses give a slightly better result. The time history of the computed E.P.W.P. is shown in Fig. 9, which includes the analytical results through the simulation under undrained condition, compared to the measured one. While the drained analysis considering pore water flow and migration well simulates the measured time history, the results obtained from the undrained analysis differ widely from the measurement irrespective of whether the effect of geometrical nonlinearity is considered or not. This is because the latter analysis can't describe the process of the dissipation of E.P.W.P., which occurs mainly after shaking, and its re-buildup due to the aftershocks following the main shock. The time history of the drained

analysis indicates that the finite strain analyses show a closer agreement including the dissipation process than the infinitesimal strain analysis except the fluctuation of E.P.W.P. during the main shock as shown in Fig. 9 (b). As mentioned above, the TL and UL formulations are equivalent to each other in terms of the E.P.W.P. response in addition to the displacement and acceleration.

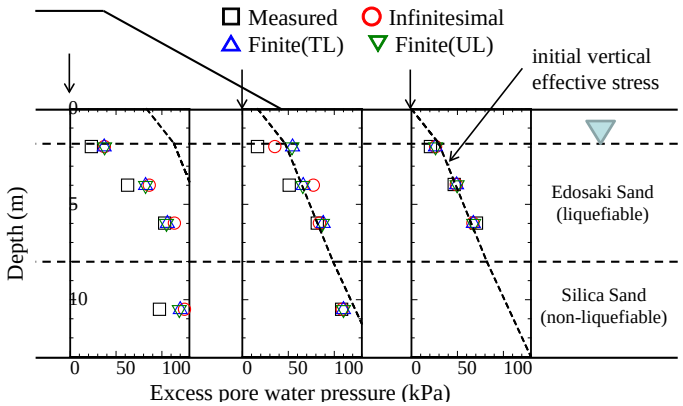

Figure 8. Variation of maximum excess pore water pressure in depth

Conclusions

In this study, the finite strain analyses are performed on the dynamic behavior of an embankment considering the effect of pore water flow and migration. The model used in the analysis is a strain space multiple mechanism model called “Cocktail glass model”, which has been extended based on finite strain formulation to take into account the effect of geometrical nonlinearity. Primary conclusions of this study are summarized as follows: 1) While the infinitesimal strain analysis overestimated the crest settlement approximately as 1.5 times as that measured, the finite strain analyses well simulated the observed deformation. 2) The time history of excess pore water pressure is well simulated by considering the pore water drainage during computation. 3) All of the computed results (e.g., settlement, acceleration, excess pore water pressure) show that the total and updated Lagrangian formulations are not only theoretically but also numerically equivalent to each other, and thereby demonstrate the validity of the program for finite strain analysis. In order to accurately predict the amount of deformation of embankments especially

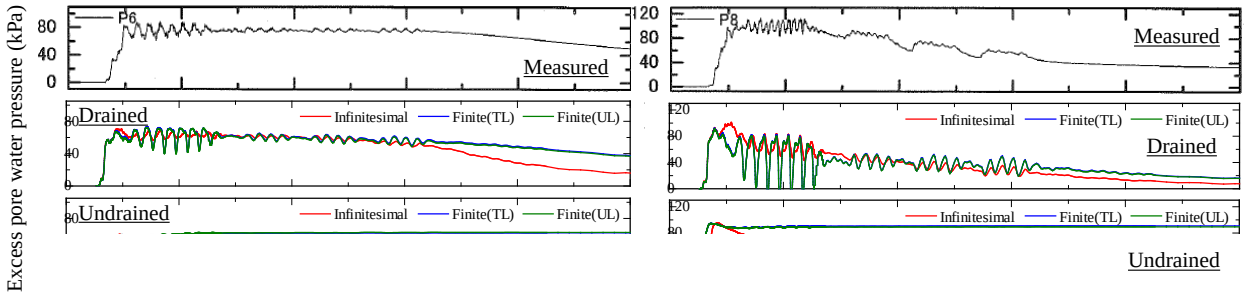

(a) 27 m from the left boundary (depth 6.5 m) (b) 33 m from the left boundary (depth 6.5 m)

Figure 9. Time history of excess pore water pressure

during a long-duration earthquake including aftershocks, it is required to take into account not only the effect of geometrical nonlinearity but also that of pore water flow and migration.

References

Hyodo, J., Iai, S., Yokoyama, N., Ozutsumi, O., and Yoshikawa, S. Effective Stress Analysis Considering Steady State of Sandy Soil on Centrifuge Model Test, *The 43rd JGS National Conference*, 1807-1808, 2008. (in Japanese)

Iai,S., Tobita,T., Ozutsumi,O. and Ueda, K. Dilatancy of Granular Materials in a Strain Space Multiple Mechanism Model, *International Journal for Numerical and Analytical Methods in Geomechanics*, Vol. **35** (3), 360-392, 2011.

Iai,S., Ueda,K., Tobita,T. and Ozutsumi, O. Finite Strain Formulation of a Strain Space Multiple Mechanism Model for Granular Materials, *International Journal for Numerical and Analytical Methods in Geomechanics*, Vol. **37** (9), 1189-1212, 2013.

Motoshima, K., Iai, S., Yokoyama, N., and Sawada, S. Influence of Fine Fraction Content, Void Ratio, etc. to the Steady State of Sandy Soil, The *43rd JGS National Conference*, 1799-1800, 2008. (in Japanese)

Public Works Research Institute *An Experimental Study on the Effects of Remedial Measure for Embankment Failure due to Earthquake-induced Foundation Liquefaction*, Technical Note, No.**3688**, 2000. (in Japanese)

Ueda, K. *Finite Strain Formulation of a Strain Space Multiple Mechanism Model for Granular Materials and its application*, Doctoral Thesis, Kyoto University, Japan, 2009 (in Japanese).

Ueda, K., Izawa, J., Murono, Y., and Iai, S. Analytical Study on the Influence of Aftershocks on the Liquefaction Behabior of Ground, *Journal of JSCE*, A1, Vol. **70**, No. 4, 578-585, 2014. (in Japanese)

Yoshizawa, M., Sakai, H., and Uzuoka, R. Applicability of Effective Stress Analysis to Seismic Assessment for River Dike during a Long-time-duration-earthquake, *Journal of structural engineering*, Vol. **55A**, 415-420, 2009. (in Japanese)

Zienkiewicz, O. C., and Bettess, P. Soil and Other Saturated Media under Transient, Dynamic Conditions*;* General Formulation and the Validity Various Simplifying Assumptions, *Soil Mechanics – Transient and Cyclic Loads*, John Wiley & Sons, 1-16, 1982.